Full Wave Analysis of Microstrip Floating Line Structures by Wavelet Expansion Method

Gaofeng Wang and Guang-Wen Pan, *Senior Member, IEEE*

Abstract— **A full wave analysis of microstrip floating line structures by wavelet expansion method is presented. The surface integral equation developed from a dyadic Green's function is solved by Galerkin's method, with the integral kernel and the unknown current expanded in terms of orthogonal wavelets. Using the orthonormal wavelets (and scaling functions) with compact support as basis functions and weighting functions, the integral equation is converted into a set of linear algebraic equations, with the matrices nearly diagonal or block-diagonal due to the localization, orthogonality, and cancellation properties of the orthogonal wavelets. Limitations inherited in the traditional orthogonal basis systems are released: The problem-dependent normal modes have been replaced by the problem-independent wavelets, preserving the orthogonality; the trade-off between orthogonality and continuity (e.g. subsectional basis functions including pulse functions, roof-top functions, piecewise sinusoidal functions, etc.) is well balanced by the orthogonal wavelets. Numerical results are compared with measurements and previous published data with good agreement.**

I. Motivation

GALERKIN'S method is a zero residual method if the basis functions are orthogonal and complete, and thus Galerkin's method with orthogonal basis functions are generally more accurate and rapidly convergent [1]. Two types of orthogonal basis functions are frequently utilized for electromagnetic field computation. Mode expansion method (or mode-matching method) has often been applied to solve scattering problems due to various discontinuities in waveguides [2], [3], finlines [4] and microstrip lines [5]. Generally, this technique is useful when the geometry of the structure can be identified as two or more regions, each of them belonging to a separable coordinate system. The basic idea in the mode expansion procedure is to expand the unknown fields in the individual regions in terms of their respective normal modes. In fact, mode expansion method is identical to Galerkin's method using the normal mode functions as the basis functions. Quite often the normal modes are made of the classical orthogonal series systems such as trigonometrical, Legendre, Bessel, Hermite, Chebyshev, etc. Owing to the orthogonality of the normal modes, a sparse system of linear algebraic equations is expected to be generated by the mode expansion method. For general cases of arbitrary geometries and material distributions, however, the mode functions are often too difficult to be constructed.

The second class of orthogonal basis functions consists of a class of subsectional bases, each of which is defined only in a given subsection of the solution domain [6]. An advantage of the subsectional bases is the localization property, that is, each of the expansion coefficients affects the approximation of the unknown function only over a subdomain of the region of interest. Thus, often not only does it simplify the computation but also leads easily to convergent solutions. In the subsectional basis systems, generally, only partial orthogonality can be attained, i.e., only the pair of bases whose supporting regions do not overlap are orthogonal. Moreover, the higher continuity order of the constructed bases is rendered, the required supporting region is larger. Hence there exists a trade-off between the orthogonality and the continuity for the subsectional basis systems.

Even if the complete orthogonal bases with higher order continuity are hard to build, the subsectional bases with certain continuity order can be constructed widely (e.g. by using polynomial interpolation functions). Especially the finite element method [7], which has been universally applied in engineering, is a subsectional basis method. So is the boundary element method [8]. Because of the kind of orthogonality or (say) localization that exists in subsectional basis systems, the differential operator equations may yield sparse systems of linear algebraic equations by using subsectional bases. However, it is also noted that the subsectional basis systems may not necessarily convert the integral operator equations into sparse systems of linear algebraic equations.

Recently, a new category of orthogonal systems, "orthogonal wavelets", has appeared on the scene [9], [10]. In image analysis and signal processing, wavelet representations have become popular and useful tools [11]–[14] mainly due to the multiresolution analysis and the localization properties in both space and frequency domains. Orthogonal wavelets also have several properties that are fascinating for electromagnetic field computations. First, wavelets are sets of orthonormal bases of $\mathbf{L}^2(\mathbf{R})$. They are problem-independent orthogonal bases and thus are suitable for numerical computations for general cases. Second, the trade-off between the orthogonality and continuity is well balanced in orthogonal wavelet systems because now the orthogonality always holds whether the supporting regions are overlapped or not. One can build an orthogonal wavelet system with any order of continuity, expecting larger support-

Manuscript received July 6, 1993; revised March 2, 1994. This research was supported in part with funds from DARPA/ESTO under grant N00014-91-J-4030 from the Office of Naval Research and Boeing Aerospace Co. under contract 133-P771.

G. Wang was with the Department of Electrical Engineering and Computer Science, University of Wisconsin, Milwaukee, Milwaukee, WI 53201, USA. He is now with Tanner Research Inc., Pasadena, CA 91107 USA.

G. Pan is with the Department of Electrical Engineering and Computer Science, University of Wisconsin, Milwaukee, Milwaukee, WI 53201, USA.

IEEE Log Number 9406800.

ing regions as higher order of continuity is selected. Third, in addition to the advantages of the traditional orthogonal basis systems, orthogonal wavelets have a cancellation property such that there is much more certainty to yield sparse systems of linear algebraic equations [15].

Furthermore, orthogonal wavelets have localization properties in both the space and frequency domains. Therefore, the decorrelation of the expansion coefficients occurs both in the space and Fourier domains. Nevertheless, according to the theory of multigrid processing [16], one can improve convergence by operating on both fine and coarse grids to reduce both the "high-frequency" and "low-frequency" component errors between the approximate and exact solutions in contrast to the traditional way of operating only on fine grids to reduce the "high-frequency" component. The expansion with subsectional bases actually is equivalent to the expansion on the finest scale only (in fact, the pulse function is equivalent to the scaling function of Haar's bases). On the contrary, the multiresolution analysis implemented by wavelet expansion provides a multigrid method. Finally, the pyramid scheme employed in the wavelet analysis provides fast algorithms [15].

So far, most previous electromagnetic modeling work on high speed digital electronics is based on quasi-static assumptions [17]–[20]. As a result, dispersion and losses due to radiation and surface wave generated from discontinuities are not properly addressed. Advanced modeling of microstrip structures by spectral domain method [21], [22], by finite difference time domain (FDTD) [23], [24] have been reported. The surface integral equation method (SIE) with Green's functions as the integral kernels has been employed to study microstrip structures [25]–[29]. To investigate microstrip discontinuities (e.g. open-end, gap, step change, T junction, etc.), a number of subsectional modes, referred to as the piecewise sinusoidal (PWS) basis functions, are used in the vicinities of the discontinuities to model the nonuniformity of the current in these regions [26]–[29]. The SIE approach uses the exact Green's function, taking into account the space wave and surface wave, and therefore is an effective full wave analysis for microstrip structures [25].

In this paper, the full wave analysis of microstrip floating line structures is implemented by the wavelet expansion method, where a system of linear algebraic equations is obtained from the integral equation. The subsectional bases (a number of piecewise sinusoidal modes) employed in [26]–[29] are replaced by a set of orthogonal wavelets. In the numerical example, we demonstrate that while the PWS basis yields full matrix, the wavelet expansion results in a nearly diagonal or nearly block-diagonal matrix; both approaches result in very close answers. However, as the geometry of the problem becomes more complicated, and consequently the resulting matrix size increases greatly, the advantage of having nearly diagonal matrix over full matrix will be more profound.

In Section II, the orthogonal wavelet theory is reviewed briefly, followed by a summary of integral equation formulation in Section III. Section IV is dedicated to the implementation of the wavelet expansion method. Section V describes the numerical evaluation of the integrals and the results are given in Section VI.

II. Orthogonal Wavelet Theory

We shall only briefly review some results of the wavelet theory relevant to the electromagnetic modeling work. For more comprehensive discussions of the wavelets, the readers are referred to monographs and books e.g., [9], [10].

A. Multiresolution Analysis, Scaling Functions and Wavelets

Since the multiresolution analysis (MRA) provides a natural way for the understanding and construction of wavelet bases, we begin with the MRA. A multiresolution analysis consists of a nested sequence of closed subspaces $\mathbf{V}_m$. More precisely, if there is a function $\phi(x) \in \mathbf{L}^2(\mathbf{R})$, called the scaling function, such that its dilating and translating versions

$$\phi_{m,n}(x) = 2^{m/2}\phi(2^m x - n) \tag{1}$$

form an orthonormal basis of the closed subspace $\mathbf{V}_m = clos_{\mathbf{L}^2(\mathbf{R})}\{\phi_{m,n}(x)\colon n \in \mathbf{Z}\}$ for $m \in \mathbf{Z}$ (the set of integers), and the subspace $\{\mathbf{V}_m\}_{m\in\mathbf{Z}}$ satisfy the following properties

$$\cdots \subset \mathbf{V}_{-1} \subset \mathbf{V}_0 \subset \mathbf{V}_1 \subset \mathbf{V}_2 \subset \cdots \tag{2}$$

$$clos_{\mathbf{L}^2}\left(\bigcup_{m\in\mathbf{Z}} \mathbf{V}_m\right) = \mathbf{L}^2(\mathbf{R}),\ \bigcap_{m\in\mathbf{Z}} \mathbf{V}_m = \{\emptyset\} \tag{3}$$

$$f(x) \in \mathbf{V}_m \Longleftrightarrow f(2x) \in \mathbf{V}_{m+1} \tag{4}$$

then a (or an orthogonal) multiresolution analysis is generated.

Once the scaling function $\phi(x)$ is selected, one may use it to construct the "mother wavelet" $\psi(x)$. It must be chosen such that $\{\psi(x-n)\}$ form an orthonormal basis of the orthogonal complementary subspace $\mathbf{W}_0$ of $\mathbf{V}_0$ in $\mathbf{V}_1$. Then its dilating and translating versions

$$\psi_{m.n}(x) = 2^{m/2}\psi(2^m x - n) \tag{5}$$

form an orthonormal basis of $\mathbf{W}_m$, the orthogonal complementary subspace of $\mathbf{V}_m$ in $\mathbf{V}_{m+1}$. Since

$$\mathbf{V}_{m+1} = \mathbf{V}_m \oplus \mathbf{W}_m \tag{6}$$

$m \in \mathbf{Z}$, from (3) it follows that

$$\bigoplus_{m\in\mathbf{Z}} \mathbf{W}_m = \mathbf{L}^2(\mathbf{R}) \tag{7}$$

and thus $\{\psi_{m,n}\}_{m,n\in\mathbf{Z}}$ is an orthonormal basis of $\mathbf{L}^2(\mathbf{R})$.

Noting $\phi(x), \psi(x) \in \mathbf{V}_1$, there exist the following expansions, called "dilation" equations

$$\phi(x) = \sum_k h_k \sqrt{2}\phi(2x-k) \tag{8}$$

$$\psi(x) = \sum_k g_k \sqrt{2}\phi(2x-k) \tag{9}$$

Once $\phi(x)$ is specified, h_k is known. It can be shown that the wavelet $\psi(x)$ can be easily generated by the last dilation equation provided that one chooses

$$g_k = (-1)^k h_{1-k} \tag{10}$$

B. Wavelet Expansion

Based on (7), any $f(x) \in \mathbf{L}^2(\mathbf{R})$ can be expanded as

$$f(x) = \sum_{m,n} \langle f(x), \psi_{m,n}(x) \rangle \psi_{m,n}(x) \tag{11}$$

where $\langle \cdot, \cdot \rangle$ represents the inner product. In practice, one often would like to approximate $f(x)$ in a subspace $\mathbf{V}_m$

$$f(x) \simeq \mathbf{A}_m f(x) \equiv \sum_n \overline{f}_{m,n} \phi_{m,n}(x) \tag{12}$$

where $\mathbf{A}_m$ is the orthogonal projection operator onto $\mathbf{V}_m$, and $\overline{f}_{m,n}$ is the inner product of $f(x)$ and $\phi_{m,n}(x)$. The orthogonal projection $\mathbf{A}_m f(x)$ is often called an approximation of the function $f(x)$ at the resolution 2^m. Equation (2) implies that the approximation of a function at resolution 2^m contains all the necessary information to compute the approximation of the same function at a lower resolution 2^{m-1}. Moreover (3) ensures that every function $f(x)$ in $\mathbf{L}^2(\mathbf{R})$ can be approximated as closely as desirable by its projection $\mathbf{A}_m f(x)$ in $\mathbf{V}_m$ and the projection will converge to the original function as m approaches ∞.

Since $\mathbf{V}_m = \mathbf{V}_{m-1} \oplus \mathbf{W}_{m-1}$, the above equation can also be written as

$$f(x) \simeq \mathbf{A}_m f(x) = \mathbf{A}_{m-1} f(x) + \mathbf{B}_{m-1} f(x) \tag{13}$$

with

$$\mathbf{B}_{m-1} f(x) \equiv \sum_n \tilde{f}_{m-1,n} \psi_{m-1,n}(x)$$

where $\mathbf{B}_{m-1}$ is the orthogonal projection operator onto $\mathbf{W}_{m-1}$, and $\tilde{f}_{m-1,n}$ is the inner product of $f(x)$ and $\psi_{m-1,n}(x)$. The above equation tells us two interesting facts. First, the approximation of $f(x)$ at the resolution 2^m contains more information than that at the resolution 2^{m-1} and the net difference is contained in the orthogonal projection $\mathbf{B}_{m-1} f(x)$ of $f(x)$ in the orthogonal complement $\mathbf{W}_{m-1}$ of $\mathbf{V}_{m-1}$ in $\mathbf{V}_m$. The difference of information between the approximations of a function at the resolutions 2^m and 2^{m-1} is called the detail function at the resolution 2^{m-1}. Secondly, by repeating this process, a more general decomposition can be obtained

$$\mathbf{A}_m f(x) = \mathbf{A}_{m_1} f(x) + \sum_{m'=m_1}^{m-1} \mathbf{B}_{m'} f(x) \tag{14}$$

where $m_1 \leq m - 1$.

Due to the special properties of multiresolution analysis, the wavelet decomposition and reconstruction can be implemented by a fast algorithm, referred to as the pyramid algorithm [11], [15].

C. 2-D Wavelet Expansion

The orthogonal wavelets can easily be extended to two-dimensional case [11], [12]. Here we only review the particular case of separable multiresolution approximations of $\mathbf{L}^2(\mathbf{R}^2)$. For such multiresolution approximations, wavelets and an MRA can be constructed from a separable function

$$\varphi(x, y) = \phi(x)\phi(y) \tag{15}$$

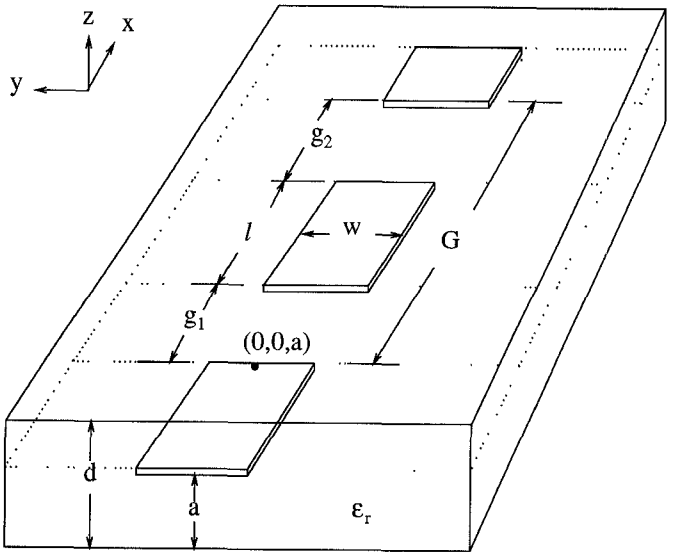

Fig. 1. Configuration of embedded floating line.

where $\phi(x)$ is a 1-D scaling function. Now there are three orthogonal wavelets associated with the scaling function $\varphi(x, y)$ in $\mathbf{L}^2(\mathbf{R}^2)$

$$\begin{aligned} \chi^{(1)}(x, y) &= \psi(x)\psi(y) \\ \chi^{(2)}(x, y) &= \psi(x)\phi(y) \\ \chi^{(3)}(x, y) &= \phi(x)\psi(y) \end{aligned} \tag{16}$$

where $\psi(x)$ is a 1-D wavelet. Almost all the properties of 1-D wavelets can be extended to the 2-D wavelets directly. Any function $P(x, x') \in \mathbf{L}^2(\mathbf{R}^2)$ can be expanded into a two-dimensional wavelet series

$$\begin{aligned} P(x, x') = \sum_{m=m_l} \sum_{n,k} & [\alpha_{n,k}^m \psi_{m,k}(x')\psi_{m,n}(x) \\ & + \beta_{n,k}^m \psi_{m,k}(x')\phi_{m,n}(x) \\ & + \gamma_{n,k}^m \phi_{m,k}(x')\psi_{m,n}(x)] \\ & + \sum_{n,k} s_{n,k}^{m_l} \phi_{m_l,k}(x')\phi_{m_l,n}(x) \end{aligned} \tag{17}$$

where $\alpha_{n,k}^m, \beta_{n,k}^m, \gamma_{n,k}^m$ and $s_{n,k}^m$ are, respectively, the inner product of $P(x, x')$ with $\psi_{m,k}(x')\psi_{m,n}(x), \psi_{m,k}(x')\phi_{m,n}(x), \phi_{m,k}(x')\psi_{m,n}(x)$ and $\phi_{m,k}(x')\phi_{m,n}(x)$. A two-dimensional version of the pyramid scheme about the wavelet coefficients $\alpha_{n,k}^m, \beta_{n,k}^m, \gamma_{n,k}^m$ and $s_{n,k}^m$ can be found in [15].

III. Basic Formulation

Fig. 1 shows the configuration of a buried microstrip floating line isolated by the two gaps from a uniform transmission line, where the substrate is assumed to extend to infinity in the transverse directions and made of a nonmagnetic, homogeneous, isotropic material of thickness d and relative permittivity ϵ_r. Both the bottom ground plane and conductor strip are considered as infinitesimally thin perfect electric conductors in the following discussions. Furthermore, for simplicity, only $\hat{\mathbf{x}}$-directed electric surface currents are assumed to flow on the

lines, which, as was found in many previous work [21], [26], is a good approximation as long as narrow lines (with respect to the wavelength) are considered.

A. Green's Function for a Grounded Dielectric Slab and the Integral Equation

The dyadic Green's function for a grounded dielectric slab and the formulation of microstrip discontinuity were derived using magnetic vector potential **A** [25], [26] or using the normal components of **E** and **H** [30], [31]. Here we only quote the relevant equations. The component of the dyadic Green's function for a grounded dielectric slab, G_{xx}, representing the $\hat{\mathbf{x}}$-component of the electric field at (x, y, a) produced by a unit $\hat{\mathbf{x}}$-directed infinitesimal dipole located at (x', y', a), can be written as [29], [32]

$$G_{xx}(x, y|x', y') = \int_{-\infty}^{\infty}\int_{-\infty}^{\infty} Q_{xx}(k_x, k_y) e^{\jmath k_x (x-x')} \cdot e^{\jmath k_y (y-y')}\, dk_x\, dk_y \tag{18}$$

where

$$Q_{xx}(k_x, k_y) = -j\frac{Z_0}{4\pi^2 \epsilon_r k_0} \cdot \left\{ (\epsilon_r k_0^2 - k_x^2)\left(\frac{k_2 \cos, [k_2(d-a)]}{T_e} + \frac{jk_1 \sin [k_2(d-a)]\}}{T_e} \right) \cdot \frac{\sin (k_2 a)}{k_2} + \frac{j(1-\epsilon_r) k_2 k_x^2 \sin^2 k_2 a)}{T_e T_m} \right\} \tag{19}$$

with

$$\begin{aligned} k_0 &= \omega\sqrt{\mu_0 \epsilon_0} \qquad Z_0 = \sqrt{\mu_0/\epsilon_0} \\ k_1^2 &= k_0^2 - k_x^2 - k_y^2; \qquad \mathrm{Im}\,(k_1) \le 0 \\ k_2^2 &= \epsilon_r k_0^2 - k_x^2 - k_y^2; \qquad \mathrm{Im}\,(k_1) \le 0 \\ T_e &= k_2 \cos (k_2 d) + jk_1 \sin (k_2 d) \\ T_m &= \epsilon_r k_1 \cos (k_2 d) + jk_2 \sin (k_2 d) \end{aligned} \tag{20}$$

As it was discussed in [25], [27], the zeros of T_e and T_m represent the TE and TM surface wave modes, respectively. T_m has always at least one zero in the whole frequency range and thus the first TM surface wave mode has no cutoff frequency [25].

The $\hat{\mathbf{x}}$-component of the electric field at $z = a$ can be formulated from the dyadic Green's function as

$$E_x(x, y) = \iint G_{xx}(x, y|x', y') I_{sx}(x', y')\, dx'\, dy' \tag{21}$$

where I_{sx} is the longitudinal electric surface current density, which only exists over all metal regions. Since the lines are assumed to be perfect conductors, an integral equation for the surface current density can be obtained by enforcing the $\hat{\mathbf{x}}$-component of the electric field on the lines to be zero

$$\iint G_{xx}(x, y|x', y') I_{sx}(x', y')\, dx'\, dy' = 0 \tag{22}$$

for $(x, y) \in S$, where S is for all the lines.

Usually, $I_{sx}(x, y)$ is written in the form of separated variables

$$I_{sx}(x, y) = I_1(x) \cdot I_2(y) \tag{23}$$

where the y-dependent factor $I_2(y)$ can be assumed as some known real functions. For example, $I_2(y)$ was chosen as a function $1 + |2y/w|^3$ to model the edge effect of the $\hat{\mathbf{x}}$-direction current distribution along the $\hat{\mathbf{y}}$-dimension [28], [29]. Substituting the expressions (18) and (23) of G_{xx} and I_{sx} into integral (22), multiplying the equation by $I_2(y)$ and integrating the result with respect to y, yield an integral equation about $I_1(x)$ as

$$\int P_{xx}(x, x') I_1(x')\, dx' = 0 \tag{24}$$

where the kernel

$$P_{xx}(x, x') = \int_{-\infty}^{\infty}\int_{-\infty}^{\infty} Q_{xx}(k_x, k_y) |F_y(k_y)|^2 \cdot e^{\jmath k_x (x-x')}\, dk_x\, dk_y \tag{25}$$

The Fourier transform $F_y(k_y)$ of $I_2(y)$ is given by

$$F_y(k_y) = \int I_2(y) e^{-\jmath k_y y}\, dy = \int_{-(w/2)}^{(w/2)} I_2(y) e^{-\jmath k_y y}\, dy \tag{26}$$

B. Current Distributions

The total region under consideration consists of three subregions incident region, transient region and transmitting region: In the incident region, the current density is approximated as the sum of incident and reflected waves, since the discontinuities are far away and the effect of discontinuities is negligible. Similarly in the transmitting region the current density is expressed by transmitted waves. In the transient region, the current density is nonuniformly distributed along the line under the influence of the discontinuities. Correspondingly, the (x-dependent factor of $\hat{\mathbf{x}}$-directed) electric surface current densities consist of four different terms: the incident, reflected, transmitted traveling waves $I^{inc}(x), I^{ref}(x), I^{tr}(x)$ and a term $I^{loc}(x)$ which is defined in the transient region (vicinity of the discontinuities) and is used to model the nonuniform current there. Mathematically

$$I_1(x) = \begin{cases} I^{inc}(x) + I^{ref}(x), & -\infty < x < -L \\ I^{loc}(x), & -L \le x \le G + L \\ I^{tr}(x), & G + L < x < \infty \end{cases} \tag{27}$$

where $G = g_1 + l + g_2$; g_1 and g_2 are respectively the width of gap 1 and gap 2; l is the length of the floating line. L is a large enough real number that the effect of discontinuities is negligible beyond $x < -L$ or $x > G + L$.

Suppose that the incident wave is propagating along $\hat{\mathbf{x}}$ direction, one can write the incident electric current as

$$I^{inc}(x) = e^{-\jmath k_e x}, \tag{28}$$

the reflected electric current as

$$I^{ref}(x) = -Re^{jk_e x}, \tag{29}$$

and the transmitted electric current as

$$I^{tr}(x) = Te^{-jk_e(x-G)} \tag{30}$$

where R and T are the reflection and transmission coefficients, respectively; k_e is the effective propagation constant of the uniform infinite microstrip line, which can easily be evaluated (e.g. see [26]-[29]). Moreover, I^{loc} can be written as

$$I^{loc}(x) = I_0(x) + I(x) \tag{31}$$

where

$$I_0(x) = \begin{cases} \left[(1-R)f_s\left(k_e x + \frac{\pi}{2}\right) - j(1+R)f_s(k_e x)\right], \\ \qquad -L \le x \le 0 \\ T\left[f_s\left(k_e[G-x] + \frac{\pi}{2}\right) + jf_s(k_e[G-x])\right], \\ \qquad G \le x \le G+L \\ 0, \qquad \text{elsewhere} \end{cases}$$

$$f_s(u) = \begin{cases} \sin u, & u < 0 \\ 0 \quad , & \text{otherwise} \end{cases}$$

Since the continuity condition must be satisfied by electric surface currents at the interfaces of the uniform current regions and transient region and the electric surface currents must be zero outside the lines, $I(x)$ is required to meet the homogeneous conditions

$$I(-L) = I(G+L) = I(x)|_{0 \le x \le g_1} = I(x)|_{g_1+l \le x \le G} = 0 \tag{32}$$

By solving integral (24) with condition (32), one can obtain reflection coefficient R, transmission coefficient T and the surface current distribution $I(x), I^{loc}(x)$ and $I_1(x)$. In the next section the wavelet bases satisfying (32) will be introduced to expand the current density $I(x)$ in the transient region.

IV. Wavelet Expansion and Matrix Equation

In this section, integral (24) is converted into a matrix equation by using wavelet expansion technique.

A. Wavelet Expansions of Unknown Function and Kernel

Since computers and physical systems only have finite precision, the exact functions are, in practice, represented by their approximations at certain resolution or precision. Based on the orthogonal wavelet theory in Section II, the projection $\mathbf{A}_m I(x)$ of the unknown function $I(x)$ on the subspace $\mathbf{V}_m$ provides an approximation at resolution 2^m and the function $I(x)$ can be approximated as closely as desirable by its projection $\mathbf{A}_m I(x)$ as m increases. Let 2^{m_h} be the resolution at which the projection $\mathbf{A}_{m_h} I(x)$ gives a sufficiently accurate approximation to $I(x)$. In the subspace $\mathbf{V}_{m_h}$, a unique expansion (approximation) can be obtained as

$$I(x) \cong \mathbf{A}_{m_h} I(x) = \sum_n \overline{I}_{m_h,n} \phi_{m_h,n}(x) \tag{33}$$

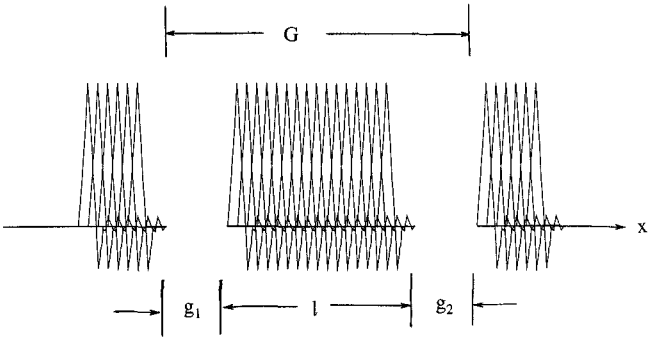

Fig. 2. Layout of scaling functions (in $\mathbf{V}_{m_h}$) on floating line.

where $\phi_{m_h,n}(x)$ is the scaling function in $\mathbf{V}_{m_h}$. Since $I(x)$ is only defined on the conductors in the transient region, that is, the intervals $[-L, 0], [g_1, g_1 + l]$ and $[G, G + L]$, the scaling function beyond these three intervals should be deleted at the boundaries. However it may lead to a solution that is difficult to satisfy the condition (32). By using compactly supported wavelets [33], one can easily delete the scaling functions that are out of the regions of interest. As a consequence, condition (32) is automatically satisfied. Fig. 2 sketches the layout of scaling functions on the floating line, the incoming and outgoing transmission lines in the vicinity of the two gaps.

To exercise the cancellation property of a wavelet basis, the above expansion about the scaling function is further converted to a wavelet expansion through a multiresolution analysis

$$\begin{aligned} I(x) &\cong \mathbf{A}_{m_h} I(x) \\ &= \sum_{m=m_l}^{m_h-1} \sum_n \tilde{I}_{m,n} \psi_{m,n}(x) \\ &\quad + \sum_n \overline{I}_{m_l,n} \phi_{m_l,n}(x) \end{aligned} \tag{34}$$

where $\psi_{m,n}(x)$ is the wavelet function of $\mathbf{W}_m$ and $m_l \le m_h - 1$.

Next, we expand the kernel in integral (24) as a two-variable function in the two-dimensional wavelet series

$$\begin{aligned} P_{xx}(x,x') = &\sum_{m=m_l} \sum_{n,k} [\alpha^m_{n,k} \psi_{m,k}(x') \psi_{m,n}(x) \\ &+ \beta^m_{n,k} \psi_{m,k}(x') \phi_{m,n}(x) \\ &+ \gamma^m_{n,k} \phi_{m,k}(x') \psi_{m,n}(x)] \\ &+ \sum_{n,k} s^{m_l}_{n,k} \phi_{m_l,k}(x') \phi_{m_l,n}(x) \end{aligned} \tag{35}$$

where $\alpha^m_{n,k}, \beta^m_{n,k}, \gamma^m_{n,k}$ and $s^m_{n,k}$ are the two-dimensional wavelet coefficients defined by the inner product of $P_{xx}(x,x')$ with $\psi_{m,k}(x')\psi_{m,n}(x), \psi_{m,k}(x')\phi_{m,n}(x), \phi_{m,k}(x')\psi_{m,n}(x)$ and $\phi_{m,k}(x')\phi_{m,n}(x)$, respectively. Since $\mathbf{V}_m = \mathbf{W}_{m-1} \oplus \cdots \oplus \mathbf{W}_{m_l} \oplus \mathbf{V}_{m_l}$ for any $m \ge m_l + 1$, the scaling function $\phi_{m,n}(x) \in \mathbf{V}_m$ can be expanded in terms of the wavelet functions $\{\psi_{m',n'}(x)\}_{m'=m-1,\cdots,m_l; n' \in \mathbf{Z}}$ and the scaling functions $\{\phi_{m_l,n'}(x)\}_{n' \in \mathbf{Z}}$. Hence, the above 2-D wavelet

expansion can also be written in the following form

$$P_{xx}(x,x') = \sum_{m,\imath=m_l-1} \sum_{n,k} P_{n,k}^{(m,i)} \tilde{\psi}_{i,k}(x') \tilde{\psi}_{m,n}(x) \quad (36)$$

where $\tilde{\psi}_{m,n}(x)$ is defined

$$\tilde{\psi}_{m,n}(x) = \begin{cases} \psi_{m,n}(x) & \text{for } m \geq m_l \\ \phi_{m_l,n}(x) & \text{for } m = m_l - 1 \end{cases}$$

and

$$\begin{aligned} P_{n,k}^{(m,\imath)} &= \langle P_{xx}(x,x'), \tilde{\psi}_{\imath,k}(x') \tilde{\psi}_{m,n}(x) \rangle \\ &= \int_{-\infty}^{\infty} \int_{-\infty}^{\infty} P_{xx}(x,x') \tilde{\psi}_{\imath,k}(x') \tilde{\psi}_{m,n}(x)\, dx'\, dx \end{aligned} \quad (37)$$

Usually (35) and (36) are, respectively, referred to the non-standard form and standard form [10], [15]. There exists a relation between the coefficients $P_{n,k}^{(m,\imath)}$ of standard form and the coefficients $\alpha_{n,k}^m, \beta_{n,k}^m, \gamma_{n,k}^m$ and $s_{n,k}^m$ of non-standard form [32]. Using the notation of $\tilde{\psi}_{m,n}(x)$, and setting $I_{m,n} = \tilde{I}_{m,n}$ if $m \geq m_l$ and $I_{m_l-1,n} = \overline{I}_{m_l,n}$, one can then rewrite (34) as

$$I(x) \cong \mathbf{A}_{m_h} I(x) = \sum_{m=m_l-1}^{m_h-1} \sum_{n} I_{m\,n} \tilde{\psi}_{m,n}(x) \quad (38)$$

For ease of notation, ordering and counting the wavelet bases in (36) and (38), and replacing double subscripts (i,k) and (m,n) by their counting number l and q respectively, one can then write (36) and (38) as

$$P_{xx}(x,x') = \sum_{q,l} P_{q,l} \tilde{\psi}_l(x') \tilde{\psi}_q(x) \quad (39)$$

and

$$I(x) \cong \mathbf{A}_{m_h} I(x) = \sum_{q=1}^{M} I_q \tilde{\psi}_q(x) \quad (40)$$

where M is the total number of basis functions in (38). Equation (40) gives an approximation of $I(x)$ in the subspace $\mathbf{V}_{m_h}$. Notice that Daubechies' scaling function of support width $2N-1$ gives rise to a wavelet whose expansions are Nth-order convergent [34], thus the truncation error $||I(x) - \mathbf{A}_{m_h} I(x)||$ of the approximation $\mathbf{A}_{m_h} I(x)$ to $I(x)$ is bounded as follows

$$||I(x) - \mathbf{A}_{m_h} I(x)|| \leq C 2^{-m_h N}$$

where C is some positive constant.

B. Matrix Equation

Substitution of (27) and (31) in (24) leads to

$$\begin{aligned} &\int_{-L}^{G+L} P_{xx}(x,x') I(x')\, dx' + R[-F^{(\imath rc)}(x) - jF^{(\imath rs)}(x)] \\ &\quad + T[F^{(trc)}(x) + jF^{(trs)}(x)] \\ &= [-F^{(\imath rc)}(x) + jF^{(\imath rs)}(x)] \end{aligned} \quad (41)$$

where

$$\begin{aligned} F^{(\imath rc)}(x) &= \int_{-\infty}^{\infty} P_{xx}(x,x') f_s\left(k_e x' + \frac{\pi}{2}\right) dx' \\ F^{(\imath rs)}(x) &= \int_{-\infty}^{\infty} P_{xx}(x,x') f_s(k_e x')\, dx' \\ F^{(trc)}(x) &= \int_{-\infty}^{\infty} P_{xx}(x,x') f_s\left(k_e[G-x'] + \frac{\pi}{2}\right) dx' \\ F^{(trs)}(x) &= \int_{-\infty}^{\infty} P_{xx}(x,x') f_s(k_e[G-x'])\, dx' \end{aligned}$$

Replacing $P_{xx}(x,x')$ and $I(x)$ in (41) by their wavelet expansions and multiplying $\tilde{\psi}_q(x)$ both sides and integrating with respect to x, one obtains

$$\sum_{l=1}^{M} P_{q,l} I_l + R P_{q,M+1} + T P_{q,M+2} = B_q \quad (42)$$

for $q = 1, 2, \cdots, M+2$, where the orthogonality $\langle \tilde{\psi}_q(x), \tilde{\psi}_l(x) \rangle = \delta_{ql}$ has been used, and

$$\begin{aligned} P_{q,l} &= \int_{-\infty}^{\infty} \int_{-\infty}^{\infty} P_{xx}(x,x') \tilde{\psi}_l(x') \tilde{\psi}_q(x)\, dx'\, dx \\ P_{q,M+1} &= -F_q^{(\imath rc)} - jF_q^{(\imath rs)} \\ P_{q,M+2} &= F_q^{(trc)} + jF_q^{(trs)} \\ B_q &= -F_q^{(\imath rc)} + jF_q^{(\imath rs)} \\ F_q^{(let)} &= \int_{-\infty}^{\infty} F^{(let)}(x) \tilde{\psi}_q(x)\, dx \\ &\qquad (\text{let} = \imath rc, \imath rs, trc, trs) \end{aligned}$$

$P_{q,l}, F_q^{(\imath rc)}, F_q^{(\imath rs)}, F_q^{(trc)}$ and $F_q^{(trs)}$ can be evaluated numerically. Equation (42) is the matrix equation for the unknown coefficients $R, T, I_1, I_2, \cdots, I_M$. The evaluation of the matrix elements involves the rigorous dyadic Green's function as a kernel. The intractable behavior of this Green's function, including singularities and strong oscillations, makes the computation of the expansion of the kernel in terms of wavelets very sensitive to the numerical treatment. The numerical aspects of expanding the kernel is described in the next section.

V. Computations of Sommerfeld-Type Integrals

The evaluation of the elements $P_{q,l}, F_q^{(\imath rc)}, F_q^{(\imath rs)}, F_q^{(trc)}$ and $F_q^{(trs)}$ is essentially to compute the Sommerfeld-type integral

$$P = \int_{-\infty}^{\infty} \int_{-\infty}^{\infty} P_{xx}(x,x') f_2(x') f_1(x)\, dx'\, dx \quad (43)$$

where $f_1(x)$ is a wavelet basis, while $f_2(x')$ can be either a wavelet basis or a function related to $f_s(\cdot)$ defined in Section III. Substituting expression (25) of P_{xx} in (43) leads to

$$\begin{aligned} P = 4 &\int_0^{\infty} \int_0^{\infty} Q_{xx}(k_x,k_y) |F_y(k_y)|^2 \\ &\cdot \Re\{F_2(k_x) F_1^*(k_x)\}\, dk_x\, dk_y \end{aligned} \quad (44)$$

where superscript $*$ and the symbol $\Re$ indicate, respectively, the complex conjugate and the real part of a complex quantity,

and

$$F_q(k_x) = \int_{-\infty}^{\infty} f_q(x) e^{-jk_x x}\, dx \tag{45}$$

where $q = 1$ or 2. Equation (44) is a spectral domain formulation.

The poles of Q_{xx} come from zeros of the T_e and T_m functions, and represent the TE and TM surface waves, respectively. Moreover, T_m has always at least one zero in the whole frequency range, indicating that the first TM surface wave mode has no cutoff frequency [25]. There are many techniques which can be used for treating the singularities caused by those TE and TM poles, including the contour deformation approach, the folding technique, the pole extraction method and so on [25]. Here, a pole extraction technique in junction with the conventional folding method was used [28].

Although the singularities related to the zeros of T_e and T_m were readily treated, the integral in (44) has two other difficulties: (1) very slow convergence; (2) rapid oscillation of the integrand for large $\beta = \sqrt{k_x^2 + k_y^2}$. The two difficulties are the consequence of the following facts that the Green's function (18) does not contain an explicit $1/R$ dependence for the decay of the fields from the source and its image; this range dependence (representing the source and image singularities) must be synthesized by the continuous spectrum of plane waves. This is the nature of the spectrum representation.

Fortunately, the source and image singularities can be shown to be identical to the singularities arising from the same source in a grounded homogeneous medium of relative permittivity

$$\epsilon_e = \begin{cases} \dfrac{\epsilon_r + 1}{2} & a = d \\ \epsilon_r & a < d \end{cases}$$

(see [27], [32]). The fields from this source and its image in the homogeneous medium can be evaluated in closed-form. Thus, it is possible to separate off the source and image singularities in closed-form from the Green's function for a grounded dielectric slab, yielding the remaining integral relatively well-behaved.

The component of the Green's function for a grounded homogeneous medium of relative permittivity ϵ_e, G_{xx}^h, representing the $\hat{\mathbf{x}}$-component of the electric field at (x, y, a) produced by a unit $\hat{\mathbf{x}}$-directed infinitesimal dipole located at (x', y', a), has a simple closed-form expression as follows (e.g. [27])

$$G_{xx}^h(x, y|x', y') = -\frac{jZ_0}{4\pi k_0 \epsilon_e}\left(k_e^2 + \frac{\partial^2}{\partial x^2}\right) \cdot \left[\frac{e^{-jk_e R_{s0}}}{R_{s0}} - \frac{e^{-jk_e R_{i0}}}{R_{i0}}\right] \tag{46}$$

where $k_e = k_0\sqrt{\epsilon_e}$, $R_{s0} = \sqrt{(x-x')^2 + (y-y')^2}$ and $R_{i0} = \sqrt{(x-x')^2 + (y-y')^2 + (2a)^2}$. Moreover, its spectral representation can be obtained [27], [32]

$$G_{xx}^h(x, y|x', y') = \int_{-\infty}^{\infty}\int_{-\infty}^{\infty} Q_{xx}^h(k_x, k_y) \cdot e^{jk_x(x-x')} e^{jk_y(y-y')}\, dk_x\, dk_y \tag{47}$$

with

$$Q_{xx}^h(k_x, k_y) = -\frac{jZ_0}{4\pi^2 k_0} \cdot \frac{k_e^2 - k_x^2}{2j\epsilon_e k_{e1}}[1 - e^{-2jk_{e1}a}] \tag{48}$$

where $k_{e1} = \sqrt{k_e^2 - k_x^2 - k_y^2}$.

Rewrite the dielectric slab Green's function (18) as

$$G_{xx}(x, y|x', y') = G_{xx}^h(x, y|x', y') + [G_{xx}(x, y|x', y') - G_{xx}^h(x, y|x', y')] \tag{49}$$

then (44) becomes

$$P = P^h + 4\int_0^{\infty}\int_0^{\infty} [Q_{xx}(k_x, k_y) - Q_{xx}^h(k_x, k_y)] \cdot |F_y(k_y)|^2 \Re\{F_2(k_x)F_1^*(k_x)\}\, dk_x\, dk_y \tag{50}$$

where

$$P^h = \int_{-\infty}^{\infty}\int_{-\infty}^{\infty} P_{xx}^h(x, x') f_2(x') f_1(x)\, dx'\, dx \tag{51}$$

$$P_{xx}^h(x, x') = \int_{-\infty}^{\infty}\int_{-\infty}^{\infty} G_{xx}^h(x, y|x', y') \cdot I_2(y') I_2(y)\, dy'\, dy \tag{52}$$

Using (47), P_{xx}^h can also be formulated in the spectral domain

$$P_{xx}^h(x, x') = \int_{-\infty}^{\infty}\int_{-\infty}^{\infty} Q_{xx}^h(k_x, k_y)|F_y(k_y)|^2 \cdot e^{jk_x(x-x')}\, dk_x\, dk_y \tag{53}$$

and then a spectral representation of P^h is obtained as

$$P^h = 4\int_0^{\infty}\int_0^{\infty} Q_{xx}^h(k_x, k_y)|F_y(k_y)|^2 \cdot \Re\{F_2(k_x)F_1^*(k_x)\}\, dk_x\, dk_y \tag{54}$$

Since the source and image singularities in G_{xx} are identical to those in G_{xx}^h, Q_{xx} and Q_{xx}^h have the same asymptotic form for large $\beta = \sqrt{k_x^2 + k_y^2}$. Thus, the second term in (50) converges fast. To compute P^h, either (51) or (54) can be used. Because of the phases of terms $e^{jk_x(x-x')}$ in (53) and $F_2(k_x)F_1^*(k_x)$ in (54), the integrands in (53) and (54) oscillate rapidly for large $\beta = \sqrt{k_x^2 + k_y^2}$, except when x is very close to x'. On the other hand, the Green's function G_{xx}^h in (52) has singularity near point $x = x'$, but allows well convergent integration for all other x. Therefore, a scheme for evaluating P^h is designed as follows

- if the supporting regions of $f_1(x)$ and $f_2(x)$ do not overlap, use the spatial formulations (51) and (52) to compute P^h;
- if the supporting regions of $f_1(x)$ and $f_2(x)$ overlap, rewrite $f_1(x)$ as $f_1^o(x) + f_1^r(x)$ and $f_2(x)$ as $f_2^o(x) + f_2^r(x)$, where $f_1^o(x)$ and $f_2^o(x)$ share the common supporting region, while $f_1^r(x)$ and $f_2^r(x)$ are the remaining parts whose support regions do not overlap. Then,
  a) use the spectral formulation (54) to compute the contribution to P^h by $f_1^o(x)\, f_2^o(x')$;

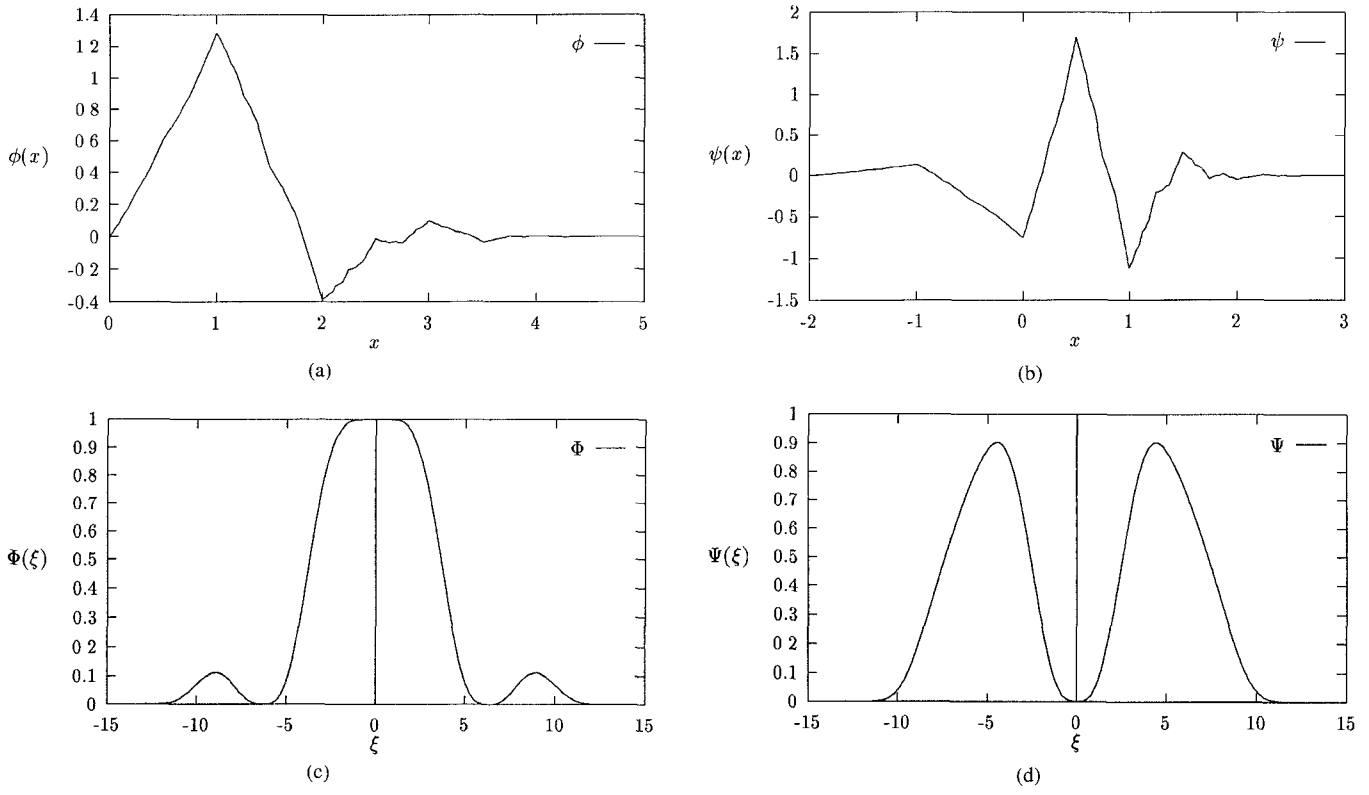

Fig. 3. Daubechies' wavelet and the Fourier transforms ($N = 3$). (a) Scaling function $\phi(x)$; (b) mother wavelet $\psi(x)$; (c) Fourier transforms $\Phi(\zeta)$ of $\phi(x)$; (d) Fourier transforms $\Psi(\zeta)$ of $\psi(x)$.

b) use the spatial formulations (51) and (52) to compute the contributions to P^h by $f_1^r(x)\, f_2^r(x')$, $f_1^r(x)\, f_2^o(x')$, and $f_1^o(x)\, f_2^r(x')$.

To calculate the infinite integrals related to $f_s(\cdot)$, we redefine $f_s(u)$ as

$$f_s(u) = \begin{cases} \sin u, & -M_s\pi < u < 0 \\ 0, & \text{otherwise} \end{cases}$$

where M_s is a large integer [26], [28]. Numerical computations demonstrated that the convergence can be achieved by setting $M_s > 6$. The infinite integrations in (51) and (52) thus become finite integrations since all $f_1(x)$, $f_2(x)$ and $I_y(x)$ now are of finite supports.

In order to use the spectral formulation, the Fourier transform of the wavelet bases must be evaluated. By using dilation (8), an iterative formulation of the Fourier transform $\Phi(\xi)$ of $\phi(x)$ is readily obtained

$$\Phi(\xi) = m_0(\xi/2)\Phi(\xi/2) \tag{55}$$

where $\Phi(0) = m_0(0) = 1$ (noting that there is a difference of a factor $1/\sqrt{2\pi}$ between the Fourier transform defined by (45) here and that in [33]), and $m_0(\xi) = 1/\sqrt{2}\,\Sigma_k\, h_k e^{-jk\xi}$. Making the use of dilation (9) and relation (10), gives the Fourier transform $\Psi(\xi)$ of $\psi(x)$ in terms of $\Phi(\xi)$

$$\Psi(\xi) = -e^{-i\xi/2} m_0^*(\xi/2 + \pi)\Phi(\xi/2). \tag{56}$$

Moreover, the Fourier transforms $\Phi_{m,n}(\xi)$ and $\Psi_{m,n}(\xi)$ of $\phi_{m,n}(x)$ and $\psi_{m,n}(x)$ can easily be shown to have the forms

$$\Phi_{m,n}(\xi) = 2^{-m/2} e^{-j\xi 2^{-m} n} \Phi(2^{-m}\xi) \tag{57}$$

$$\Psi_{m,n}(\xi) = 2^{-m/2} e^{-j\xi 2^{-m} n} \Psi(2^{-m}\xi) \tag{58}$$

Generally, the infinite integrations in (50) and (54) can be truncated at $k_x = k_y \simeq 200k_0$ with sufficient accuracy.

VI. Numerical Results and Sparsity of Impedance Matrix

A FORTRAN program was written implementing the procedure developed in the preceding sections. Daubechies' wavelets, one type of orthogonal wavelets with compact support [9], [33], are employed for our calculations. Fig. 3 illustrates Daubechies' wavelet and its Fourier transform for $N = 3$. It has been found that the convergence may speed up by adding one edge basis near each end of the conductors into the conventional wavelet basis (since the edge basis provides a better representation to match the edge current distribution). In this section, numerical results obtained from the wavelet expansion method are compared with measurements and computational results of the PWS basis functions, and the improvement of the sparsity of the impedance matrix by using the wavelets over the PWS basis is also illustrated. All of the following examples are executed on the IBM RS-6000/530, and roughly a factor of 2 in the CPU time savings of the wavelet against PWS basis were recorded. We believe that as the unknowns increase, and the matrix size grows, the advantage of using wavelet basis will be more significant.

A. Numerical Results

Example 1—Open ended microstrip transmission line: For the first example, let us consider an open ended microstrip

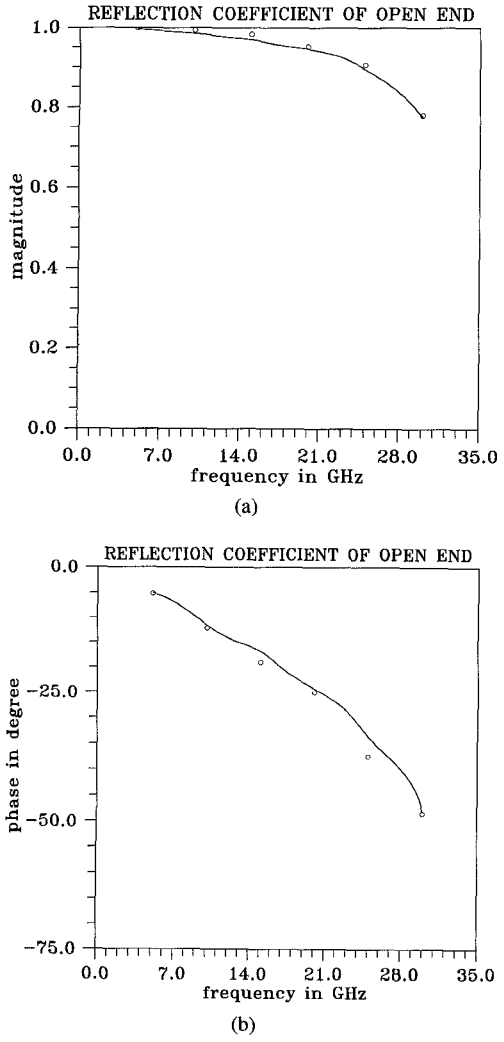

Fig. 4. Comparison of results of open ended microstrip transmission line using the wavelet expansion method and the spectral domain method and measurement. (a) Magnitude of the reflection coefficient ('solid line' wavelet. 'o o o' SDM). (b) Phase of the reflection coefficient ('solid line' wavelet, 'o o o' measurement).

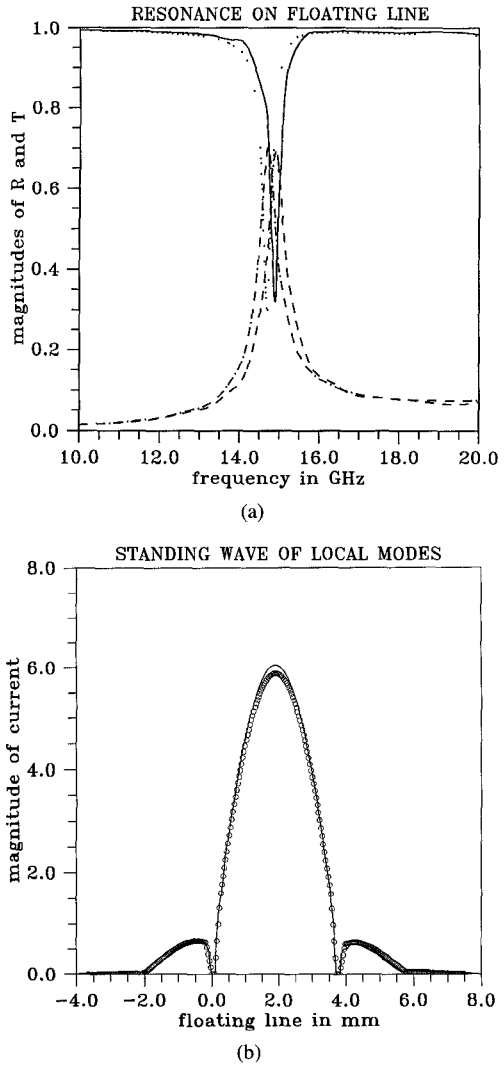

Fig. 5. Comparison of results of miocrostrip floating line resonator using this method and PWS basis functions. (a) magnitude of the reflection and transmission coefficients versus frequency ('solid line'$|R|$ from wavelet, '- - - -' $|T|$ from wavelet, '.....' $|R|$ from PWS. '- . - . -' $|T|$ from PWS). (b) Magnitude of the standing wave current on the floating line as well as the local modes on both sides of the floating line ('solid line' wavelet, 'o o o' PWS).

transmission line with $\epsilon_r = 9.90, w = 0.6$ mm and $d = 0.635$ mm. The magnitude and phase of the reflection coefficient are calculated and compared with those of the spectral domain method and measurement [22] in Figs. 4(a) and 4(b), respectively. Good agreement between our results and the measured values can be observed.

Example 2—Microstrip floating line resonator: A microstrip floating line with parameters $\epsilon_r = 8.875, \ell = 3.653$ mm, $g_1 = g_2 = 0.08$ mm and $d = a = w = 0.508$ mm (see Fig. 1) is investigated in this example. To search for the resonant frequency, the reflection and transmission coefficients are computed at different frequencies. Fig. 5(a) depicts the magnitudes of the reflection coefficient R and transmission coefficient T versus frequency as computed by this method in comparison with the calculations of the PWS basis functions [28]. The results from this method agree well with those from [28]. At the resonant frequency, the magnitude of the standing wave current on the floating line as well as the local modes on both sides of the floating line from this technique is illustrated in Fig. 5(b) against the curve obtained by using the PWS basis functions [28]. Again very good agreement between the two sets of results is demonstrated. In this example, the CPU time is about 4 hours for the PWS basis, and 2 hours for the wavelet basis.

Example 3: Embedded microstrip floating line resonator: The wavelet expansion method is also applied to a buried microstrip floating line. Given parameters in Fig. 1 as $\epsilon_r = 10.0, \ell = 14.00$ mm, $g_1 = g_2 = 0.2$ mm, $d = 0.660$ mm and $a = w = 0.560$ mm, we search for the resonant frequency. The magnitudes of the reflection coefficient R and transmission coefficient T versus frequency obtained by the wavelet expansion method is plotted in Fig. 6(a). The resonant frequency is obtained about 7.54 GHz. At the resonant frequency, the magnitude of the standing wave current on the buried floating line and the local modes on both sides of the buried floating line are depicted in Fig. 6(b).

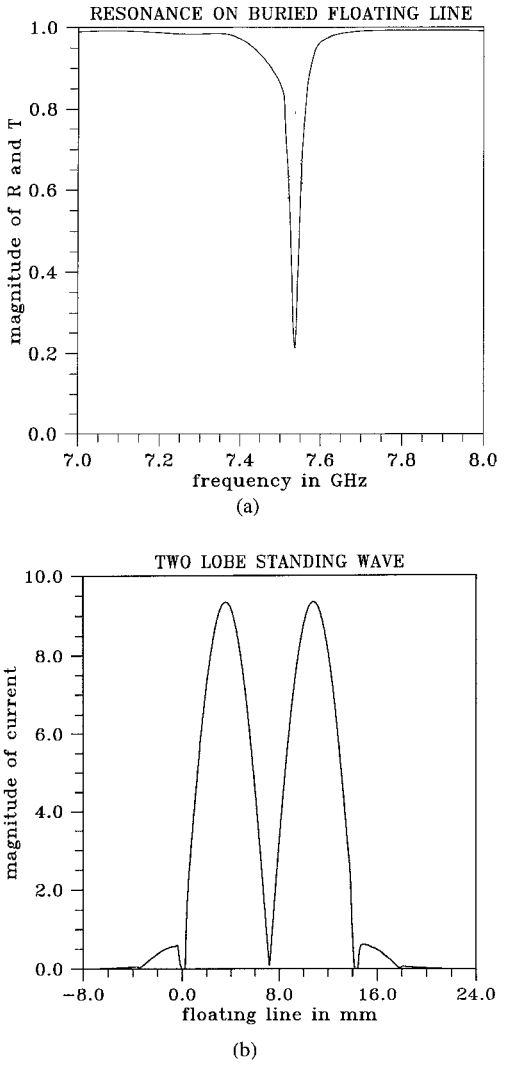

Fig. 6. Results of embedded microstrip floating line rosonator using wavelet expansion method. (a) Magnitude of the reflection and transmission coefficients versus frequency. (b) Magnitude of standing wave current on the embedded floating line as well as the local modes on both sides of the embedded floating line.

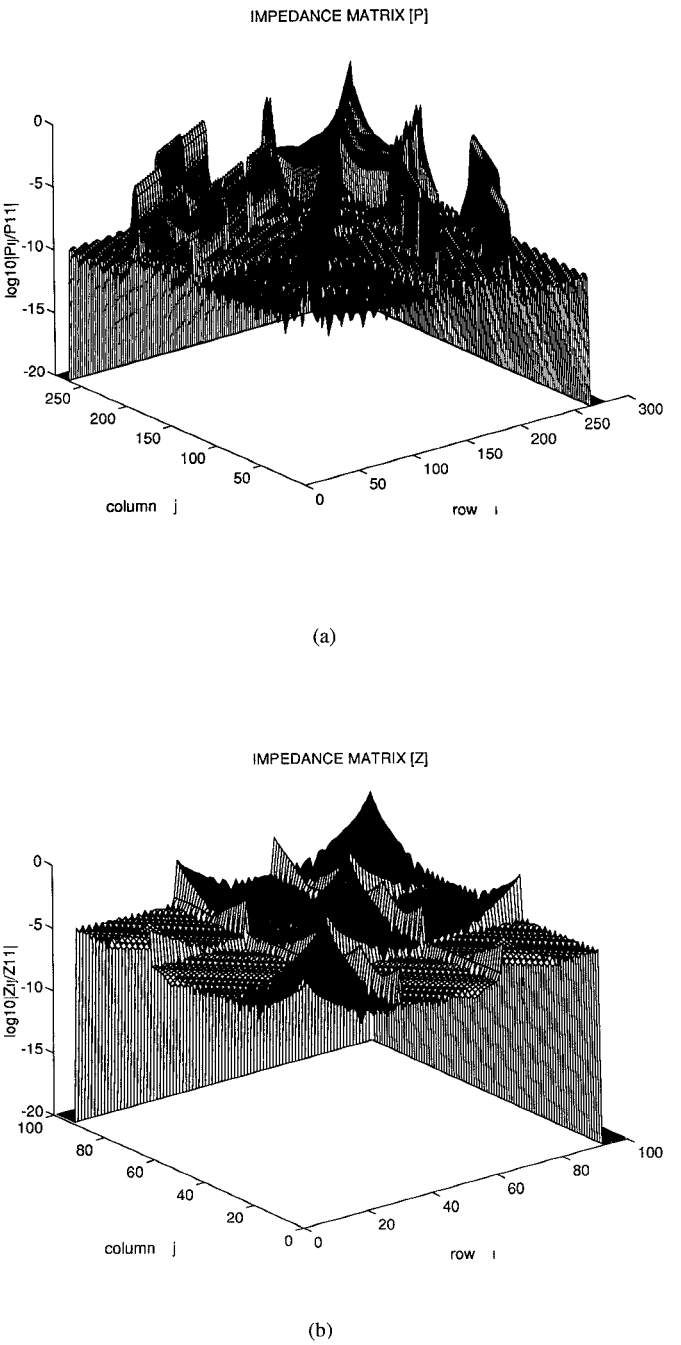

Fig. 7. Comparison of impedance matricies in the computation of the current distribution on microstrip floating line resonator using this method and PWS basis functions in example 2. (a) 3-D logarithmic plots of typical impedance matrix by using wavelets. (b) 3-D logarithmic plots of typical impedance matrix by using PWS basis functions.

Comparing this example with example 4 in [29], all parameters are the same except that the floating line in this example is about half of that in [29], and all conductor lines are 0.10 mm narrower and embedded down 0.10 mm in the substrate. There are two current lobes on the floating line here instead of four current lobes as in [29] at the resonant frequency. The resonant frequency decreases slightly from 8 GHz in [29] to 7.54 GHz here.

B. Sparsity of Impedance Matrices

As expected, the wavelet expansion method yields a sparse impedance matrix $[P_{q,l}]$. Figs. 7(a) and 7(b) illustrate, respectively, the 3-D logarithmic plots of typical normalized impedance matrices generated in example 2 by wavelet expansion method (with $m_h = 15$ and $m_l = 13$) and by the PWS basis functions [28]. It can be observed that the impedance matrix from wavelets is nearly diagonal or block-diagonal. Although the size $N = 264$ of the impedance matrix from wavelets is larger than the size $N = 92$ from PWS basis functions, the effective size from wavelets is still smaller than that from PWS basis functions due to the sparsity of the impedance matrix from wavelets. The sparseness of the matrix has even more profound significance for the problems where large matrices are generated.

In order to give a measure of sparsity in an impedance matrix, we replace each entry of a matrix by its magnitude normalized by the magnitude of the largest element. Now the

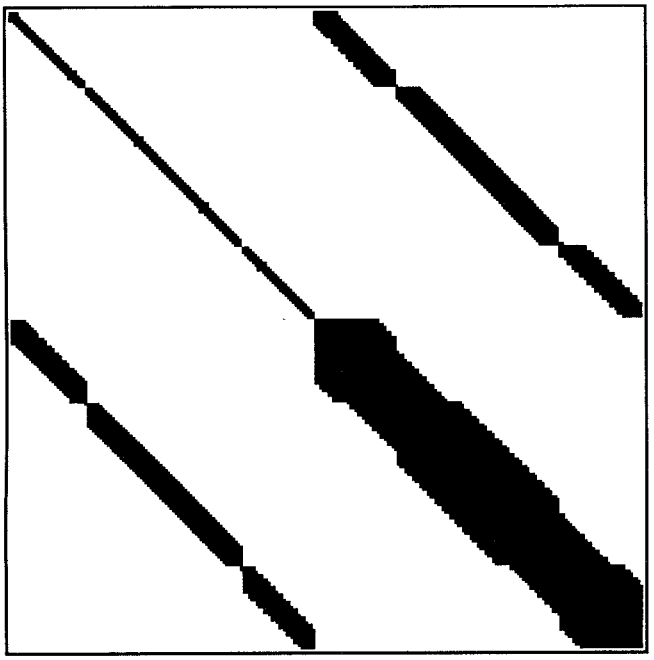

(a)

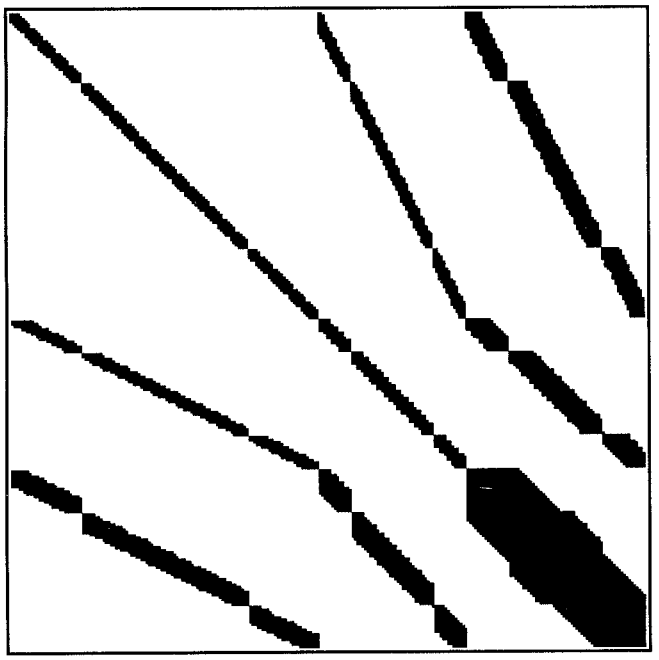

(b)

Fig. 8. Sparsity of impedance matrices in the computation of the current distribution on buried microstrip floating line resonator using this method in example 3. (a) Sparsity of typical impedance matrix with $m_h = 14$ and $m_l = 13$. (b) Sparsity of typical impedance matrix with $m_h = 14$ and $m_l = 12$.

entries below a threshold, say 10^{-6}, are set to zero, and the remaining entries are considered as the significant (non-zero) elements. The ratio of the significant entries to the total entries in the matrix measures the sparseness of the matrix. In Fig. 8(a) the black ink shows the non-zero elements of an impedance matrix in example 3 with $m_h = 14$ and $m_l = 13$. A similar result of the same problem in example 3 with more resolution levels ($m_h = 14$ and $m_l = 12$) is depicted in Fig. 8(b). In contrast, a full black square, representing a full matrix, will be plotted if the PWS basis functions are used. From Fig. 8(a) of the matrix 416×416 and Fig. 8(b) of the matrix 351×351 it can be seen that as more resolution levels are used, the dense "plateau" area of the impedance matrix shrinks. This is not surprising. As the decomposition reaches more levels, more wavelets and less scaling functions are used. The wavelets possess cancellation and localization properties in addition to the orthogonality that the scaling functions can only provide.

VII. Conclusion

In this paper, a full wave analysis of microstrip floating line structures by wavelet expansion method has been presented. Numerical results from the wavelet expansion method are compared with measurements and previous published data with good agreement. It has been demonstrated that the replacement of the PWS bases by the orthogonal wavelets with compact support can greatly improve the sparseness of the resulting matrix from the boundary integral equations, in particular for problems involving large matrices.

Acknowledgment

The authors wish to thank Dr. J. Murphy, DARPA/ESTO, Dr. R. Pohanka and Dr. L. Kabacoff, ONR, and Dr. P. Young, Boeing High Technology Center, Dr. B. Gilbert of Mayo Foundation for support and helpful discussions, and to Dr. J. Tan of University of Wisconsin-Milwaukee for the PWS results and corresponding figures.

References

[1] J. H. Wang, *Generalized Moment Methods in Electromagnetics: Formulation and Computer Solution of Integral Equations*. New York: John Wiley & Sons, 1991.

[2] A. Wexler, "Solution of waveguide discontinuities by modal analysis," *IEEE Trans. Microwave Theory Tech.*, vol. MTT-15, pp. 508–517, Sept. 1967.

[3] R. Mittra and W. W. Lee, *Analytical Techniques in the Theory of Guided Waves*. New York: Macmillan, 1971.

[4] A. S. Omar and K. Schunemann, "Transmission matrix representation of finline discontinuity," *IEEE Trans. Microwave Theory Tech.*, vol. MTT-33, pp. 765–770, Sept. 1985.

[5] T. S. Chu, T. Itoh, and Y. C. Shih, "Comparative study of mode-matching formulations for microstrip discontinuity problems," *IEEE Trans. Microwave Theory Tech.*, vol. MTT-33, pp. 1018–1023, Oct. 1985.

[6] R. F. Harrington, *Field Computation by Moment Methods*. New York: Macmillan, 1968.

[7] O. C. Zienkiewicz and K. Morgan, *Finite Elements and Approximation*. New York: John Wiley & Sons, 1983.

[8] C. A. Brebbia, *The Boundary Element Method for Engineers*. London: Pentech, 1978.

[9] I. Daubechies, *Ten Lectures on Wavelet*. Philidelphia: SIAM Press, 1992.

[10] C. K. Chui, *An Introduction to Wavelets*. New York: Academic, 1991.

[11] S. G. Mallat,"A theory for multiresolution signal decomposition: the wavelet representation," *IEEE Trans. Pattern Anal. Machine Intell.*, vol. PAMI-11, pp. 674–693, July 1990.

[12] C. K. Chui, Ed., *Wavelets—A Tutorial in Theory and Applications*. New York: Academic, 1992.

[13] M. Vetterli,"Wavelets and filter banks for discrete-time signal processing," in M. B. Ruskai, *et al*, Eds.*Wavelets and Its Applications*. Boston: Jones and Bartleth, 1992, pp. 17–52.

[14] G. Wang, J. Zhang, and G. Pan, "Solution of inverse problems in image processing by wavelet expansion," to appear *IEEE Trans. Image Processing*, May 1985.

[15] G. Beylkin, R. R. Coifman, and V. Rokhlin,"Fast wavelet transforms and numerical algorithms I," Yale University, Tech. Rep. YALEU/DCS/RR-

696, Aug. 1989, *Comm. on Pure Appl. Math.*, vol. XLIV, pp. 141–183, 1991.
[16] W. Hackbusch, *Multi-grid Methods and Applications* New York: Springer-Verlag, 1985.
[17] G. Pan, K. Olson, and B. Gilbert, "Improved algorithmic method for the prediction of wavefront propagation behavior in multiconductor transmission lines in multilayered dielectric media," *IEEE Trans. Computer-Aided Design*, vol. 8, pp. 608–621, June 1989.
[18] G. Pan, G. Wunsch, and B. Gilbert, "Frequency-domain analysis of coupled nonuniform transmission lines using Chebyshev pseudo-spatial techniques," *IEEE Trans. Microwave Theory Tech.*, vol. MTT-40, pp. 2025–2033, Nov. 1992.
[19] C. Wei, R. F. Harrington, J. R. Mautz, and T. K. Sarkar, "Multiconductor transmission lines in multilayered dielectric media," *IEEE Trans. Microwave Theory Tech.*, vol. MTT-32, pp. 439–449, Apr. 1984.
[20] G. Pan, G. Wang, and B. Gilbert, "Edge effect enforced boundary element analysis of multilayered transmission lines," *IEEE Trans. Circuits and Syst. I: Fundamental Theory and Applications*, vol. 39, no. 11, Nov. 1992.
[21] T. Itoh and R. Mittra, "Spectral-domain approach for calculating the dispersion characteristics of microstrip lines," *IEEE Trans. Microwave Theory Tech.*, vol. MTT-21, pp. 496–499, July 1973.
[22] J. Mclean, H. Ling, and T. Itoh, "Full wave modeling of electrically wide microstrip open discontinuities via a deterministic spectral domain method," *MTT-s Dig.*, vol. 2, no. 4, pp. 1155–1158, 1990.
[23] X. Zhang and K. K. Mei, "Time-domain finite difference approach to the calculation of the frequency-dependent characteristics of the microstrip discontinuities," *IEEE Trans. Microwave Theory Tech.*, vol. MTT-36, pp. 1775–1787, Dec. 1988.
[24] D. M. Sheen, S. M. Ali, M. D. Abouzahra, and J. A. Kong, "Application of the three-dimensional finite difference time-domain method to the analysis of planar microstrip circuits," *IEEE Trans. Microwave Theory Tech.*, vol. MTT-38, pp. 849–857, July 1990.
[25] J. R. Mosig and F. E. Gardiol, "A dynamical radiation model for microstrip structures," *Advances in Electron. Electron Physics*, vol. 59, New York: Academic, 1982, pp. 138–236.
[26] R. W. Jackson and D. M. Pozar,"Full-wave analysis of microstrip open-end and gap discontinuities," *IEEE Trans. Microwave Theory Tech.*, vol. MTT-33, pp. 1036–1042, Oct. 1985.
[27] D. M. Pozar, "Improved computational efficiency for the moment method solution of printed dipoles and patches," *Electromagnetics*, vol. 3, pp. 299–309, 1983.
[28] G. Pan, J. Tan, and J. Murphy, "Full-wave analysis of microstrip floating line discontinuities," *IEEE Trans. Electromagnetic Compatibility*, vol. 36, no. 1, Feb. 1994.
[29] G. Pan and J. Tan "Full-wave analysis of radiation effect of microstrip transmission lines," *Int. J. Analog Integrated Circuits and Signal Processing*, Special Issue on High-speed Interconnects, vol. 5, no. 1, Jan. 1994.
[30] J. A. Kong, *Electromagnetic Waves Theory*. New York: John Wiley & Sons, 1986.
[31] W. C. Chew, *Waves and Fields in Inhomogeneous Media*. New York: VNR, 1990
[32] G. Wang, "Numerical techniques for electromagnetic modeling of high speed circuits," Ph.D. dissertation, University of Wisconsin-Milwaukee, Oct., 1993.
[33] I. Daubechies, "Orthonormal bases of compactly supported wavelets," *Commun. Pure Appl. Math.*, vol. 41, pp. 909–996, Nov. 1988.
[34] B. K. Alpert, "Wavelets and other bases for fast numerical linear algebra," in *Wavelets: A Tutorial in Theory and Applications*. New York: Academic, C. K. Chui, Ed., 1992.

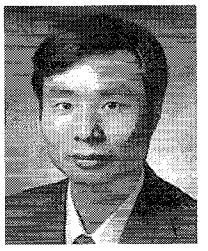

Gaofeng Wang was born in Hubei, China, December 24, 1965. He received the B.S. degree in physics from Hubei University and the M.S. degree in space and radio physics from Wuhan University, Wuhan, China, in 1983 and 1988, respectively, and the Ph.D. degree in electrical engineering with minors in mathematics and computer science from the University of Wisconsin-Milwaukee (UWM) in 1993.

From 1988 to 1990 he was with the Department of Space Physics, Wuhan University, Wuhan, China, where he was involved in research and teaching of radiowave propagation in ionosphere and numerical methods for electromagnetic waves and fields.

From 1990 to 1993 he was a graduate research assistant in the Department of Electrical Engineering and Computer Science UWM. Currently, he is a scientist at Tanner Research, Inc., Pasadena, CA. His current research interests are numerical techniques for electromagnetic modeling of high speed circuits, signal integrity analysis of electronic systems and wavelet applications in numerical analysis and image processing.

Guang-Wen (George) Pan (S'83–M'84–SM'94) received the B.E. degree in mechanical engineering from Peking Institute of Petroleum Technology in 1967. He attended the Graduate School, University of Science and Technology of China from 1978 to 1980, majoring in electrical engineering. He received the M.S. degree in 1982 (working on Pattern Recognition), and the Ph.D. degree in 1984 (working on Rough Surface Scattering) both in electrical engineering from the University of Kansas, Lawrence, KS.

He worked at the Institute of Development and Research in Northwest of China in machine design as an associate engineer, and then as an electrical engineer responsible for design of pulse-width modulation electronics and digital remote fire control systems used in petroleum seismic exploration. He came to the United States in August 1980 as a research assistant in the Remote Sensing Laboratory, University of Kansas. From September 1984 to May 1985, he was a post-doctoral fellow at the University of Texas, engaged in a project on Computer Aided Design of Airborne Antenna/Radome Systems. He joined the Mayo Foundation in 1985, engaged in the theoretical modeling of the electromagnetic behavior of high-speed integrated circuits, electronic circuit boards, and high density substrates, placement and routing.

From 1986 to 1988 he was an associate professor in the Department of Electrical Engineering, South Dakota State University. In 1988 he joined the Department of Electrical Engineering and Computer Science at the University of Wisconsin-Milwaukee as an associate professor. He has been the Director of the Signal Propagation Research Laboratory since 1990 and became a professor in 1993. His research interests continue to be in the mathematical modeling of the electromagnetic environment of high clock rate signal processors.

Dr. Pan is cited in Who's Who in the Midwest and is a member of Eta Kappa Nu.